Available online at www.sciencedirect.com
ScienceDirect
Applied Thermal Engineering 27 (2007) 1967–1977
Applied Thermal Engineering
www.elsevier.com/locate/apthermeng

Study of a new environmental chamber design

B.J. Huang *, Y.C. Liao, T.C. Kuo

Department of Mechanical Engineering, National Taiwan University, Taipei, Taiwan

Received 29 September 2006; accepted 11 December 2006
Available online 8 January 2007

Abstract

The present study develops an environmental chamber for temperature and humidity control (THCS) in which the condenser is divided into two parts. By properly adjusting the fan speeds of the outer and inner condensers, an enclosed chamber can obtain net heating or cooling effect and the temperature and humidity can be directly controlled. The system dynamics of the THCS is first studied. The temperature response models, $G_{11}(s)$ and $G_{12}(s)$, are shown to be of a first order. The humidity response models, $G_{21}(s)$ and $G_{22}(s)$, are of second order with a zero. It is found that the multiple-input-multiple-output (MIMO) control system can be decoupled into a temperature and humidity control loops. A control system using a PI controller is designed and implemented on a PC with an 8051 microprocessor. It has experimentally been shown that the chamber temperature and humidity can be controlled to within ±0.1 °C and ±1% R.H., respectively. In the presence of a heat load disturbance, the controller can restore the THCS to operate at the setting values within a reasonable transient time.

Keywords: Environmental chamber; Temperature/humidity control; Multivariable control

1. Introduction

A domestic dehumidifier usually utilizes a simple Rankine refrigeration cycle to lower the surface temperature of the evaporator heat exchanger to a value below the dew point of the room air such that the moisture of the incoming air can be removed by condensation. Air is also cooled simultaneously in the dehumidifying process. The cooled air is then used to cool the condenser and get reheated before returning to the room. The processed air becomes dry but has a temperature rise due to the energy balance of the dehumidifier. This means that the room air will be heated up during the dehumidifying process. Thus the room temperature thus cannot be controlled using this kind of dehumidifier.

When both temperature and humidity control are required in some applications, the process will include an additional reheating process, in addition to the dehumidification process ($a \rightarrow c$ as shown in Fig. 1), to heat the cooled air to a higher temperature ($c \rightarrow d$), and another humidifying process using water spray to adjust the air humidity and temperature to the desired condition ($d \rightarrow e$) before returning to the room. Basically, such a temperature and humidity control will utilize the multivariable or decoupled control technique [1–3] since temperature and humidity will interact with each other during the cooling, reheating or humidifying process. The control system is thus complicated.

A modification for the design of temperature and humidity control is proposed in the present study (see the Mollier diagram in Fig. 1). The condenser is designed in two parts. The outer condenser is installed outside a chamber or a room with a cooling fan. The inner condenser is installed inside a chamber and is connected to the evaporator. The air inside the chamber is sucked into the evaporator by a fan and then blown through the inner condenser for reheating. The re-circulated air is thus cooled and dehumidified in the evaporator first ($a \rightarrow b$). Then it is reheated

* Corresponding author. Tel.: +886 2 23634790; fax: +886 2 23640549.
E-mail address: bjhuang@seed.net.tw (B.J. Huang).

1359-4311/$ - see front matter © 2006 Elsevier Ltd. All rights reserved.
doi:10.1016/j.applthermaleng.2006.12.010

Nomenclature

E_i	voltage of the inner fan, V	Q_e	heat absorbed by the evaporator, i.e. the energy pumped out by the Rankine cycle, W
E_o	voltage of the outer fan, V	Q_L	heat loss from the chamber to the ambient due to insulation and air leakage, W
$G_{11}(s)$, $G_{12}(s)$	temperature response models	Q_s	heat generation due to a heat source inside the chamber, W
$G_{21}(s)$, $G_{22}(s)$	humidity response models	T_x	chamber temperature, °C
H_x	humidity, %R.H.	$\sim$	perturbation
M_x	mass of the chamber, kg	$\bar{}$	mean value; steady-state
Q_{ci}	heat dissipation rate of the inner condenser, W		
Q_{co}	heat dissipation of the outer condenser, W		
Q_d	heat released by sensible heat of water condensate, W		

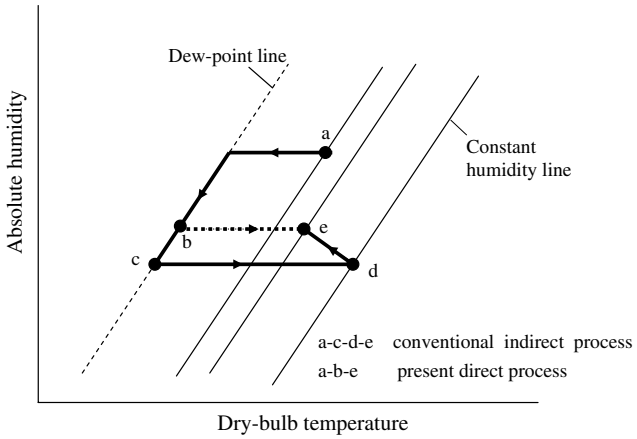

Fig. 1. Mollier diagram of the humidity/temperature control process.

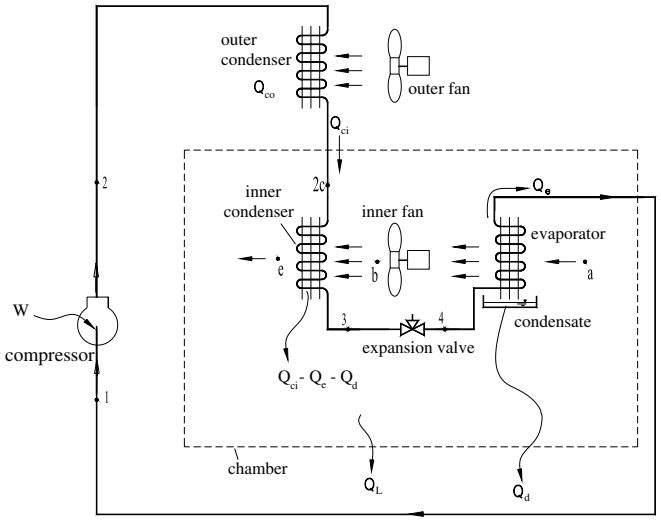

Fig. 2. Schematic diagram of the enclosed chamber with THCS.

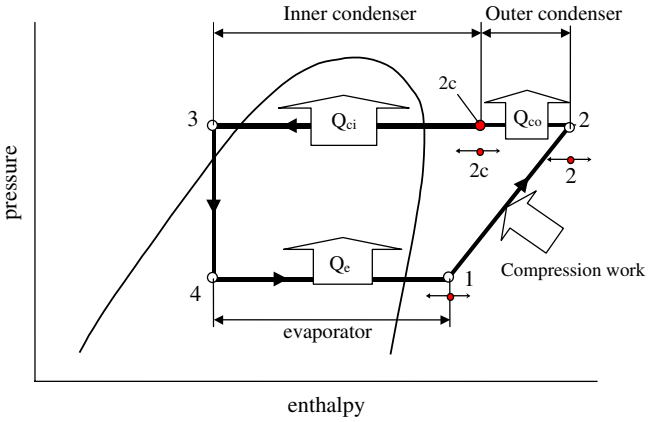

Fig. 3. Thermodynamic diagram of Rankine cycle used in the temperature and humidity control.

in the inner condenser ($b \rightarrow e$) to the desired condition (state e). By properly adjusting the fan speeds of the outer and inner condensers, the heat dissipation of the two individual condensers can be varied. Point 2c shown in the thermodynamic cycle of Fig. 3 is thus movable depending upon the fan speed. According to the energy balance for the chamber, we have

$$M_x C_v \frac{dT_x}{dt} = Q_{ci} + Q_s - Q_e - Q_L - Q_d, \quad (1)$$

where M_x is the mass of the chamber; T_x is the chamber temperature; Q_{ci} is the heat dissipation rate of the inner condenser; Q_s is the heat generation due to a heat source inside the chamber; Q_e is the heat absorbed by the evaporator, i.e. the energy pumped out by the Rankine cycle; Q_L is the heat loss from the chamber to the ambient due to insulation and air leakage etc; and Q_d is the heat released by sensible heat of the water condensate.

From Fig. 2, the thermodynamic state 2c determines the heat capacity of the two condensers. State 2c to state 3 represents the heat dissipation of the inner condenser Q_{ci}. State 2 to state 2c represent the heat dissipation of the outer condenser Q_{co}. State 4 to state 1 is the heat absorbed by the evaporator.

Reducing the fan speed of the outer condenser will cause the heat dissipation of the outer condenser Q_{co} to decrease and both Q_{ci} and Q_e will increase with increasing fan speed of the inner condenser. States 1, 2 and 2c are thus movable by changing the speed of the two fans as seen from Fig. 3. Therefore, the chamber temperature can be increased if the following condition exists:

$$Q_{ci} + Q_s > Q_e + Q_L + Q_d, \quad (2)$$

The chamber temperature can be decreased if the following condition exists:

$$Q_{ci} + Q_s < Q_e + Q_L + Q_d. \quad (3)$$

Hence, the net heating or cooling of the chamber and the temperature and humidity control can be achieved by adjusting the fan speed. The temperature and humidity control of the present design thus follows a direct process $a \to b \to e$ as shown in Fig. 1. Fig. 1 is the comparison of the Mollier diagrams for the conventional indirect control process ($a \to c \to d \to e$) and the present direct process ($a \to b \to e$). It can be seen that the present direct control process is simple and the energy consumption will be low. The present study intends to develop such a direct temperature and humidity control system (THCS) based on the above operating principle for an enclosed chamber.

2. Control system design principle

Fig. 4 is the information-flow diagram which expresses the information flow of the THCS. The THCS is a multiple-input-multiple-output (MIMO) dynamic system. The system outputs consist of temperature (T_x) and humidity (H_x) of the chamber. The manipulatable inputs of the system consists of the input voltage of the inner and outer fans, E_i and E_o, respectively. The disturbance inputs include the ambient air temperature T_a, the heat loss Q_L, the water condensate heat release Q_d. The system is thus a 2×2 MIMO system.

The control of a MIMO system is quite complicated due to the interacting or the cross effect between inputs and outputs. The transfer function of the THCS can be expressed as a 2×2 matrix shown in Eq. (4).

$$G(s) \equiv \frac{Y(s)}{U(s)} = \begin{bmatrix} G_{11}(s) & G_{12}(s) \\ G_{21}(s) & G_{22}(s) \end{bmatrix}, \quad (4)$$

$$\text{where } Y(s) = \begin{bmatrix} T_x(s) \\ H_x(s) \end{bmatrix}, \quad U(s) = \begin{bmatrix} E_i(s) \\ E_o(s) \end{bmatrix}.$$

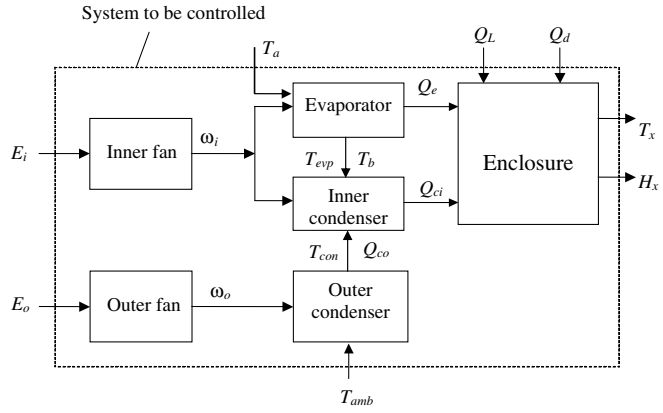

Fig. 4. Information diagram of the system.

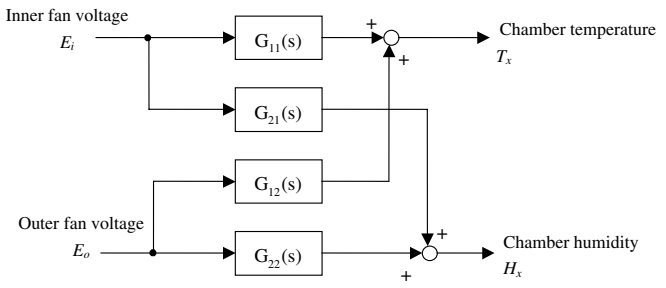

Fig. 5. Interacting or cross effect of THCS.

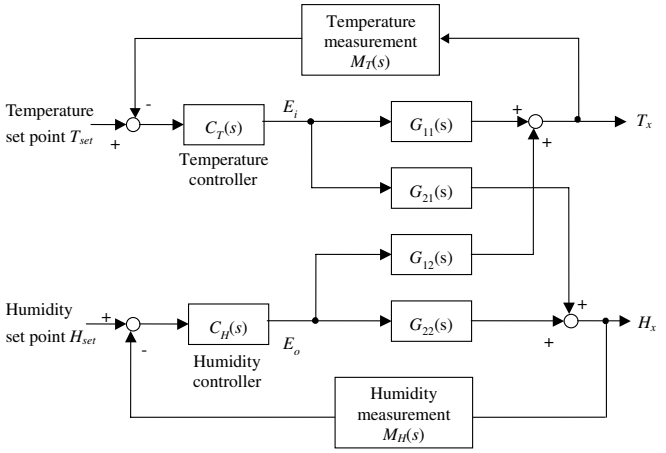

Fig. 6. Configuration of the feedback control system for THCS.

The system block diagram in Fig. 5 which shows the interaction between the inputs and the outputs. The chamber temperature T_x and humidity H_x are affected by the input voltages of the inner and outer fans, E_i and E_o. The block diagram of the control system for the THCS is as shown in Fig. 6.

Some methods are used to treat the process control of a MIMO system with interaction effects, such as the decoupling method [1,4]. For the present THCS, we will identify the system dynamics model of the MIMO system first. If the cross effect of either $G_{12}(s)$ or $G_{21}(s)$ is negligible, i.e. the control system is half-coupled, we can then separate the whole feedback control loop into two individual feedback loops. The controllers can then be designed separately. The system identification for the THCS is thus carried out first for a prototype.

3. System identification of a THCS

3.1. Hardware design of a THCS

A THCS is designed in the present study. A chamber that is retrofitted from a domestic refrigerator with an interior volume of 80 l (outside dimension $69 \times 44 \times 49$ cm) is used. The components of the Rankine cycle machine consist of an R134a compressor (TECUMSEH AZ3414Y, 250 W input), and two fan-coil heat exchangers (300 W) that act as the inner and outer condensers. The inner fan

is a 12 V DC-powered 119×119 mm fan (SANYO 109R1212H102) with a 3.84 W input. The outer fan is also a 12 V DC-powered 119×119 mm fan TOSHIBA D12H1205A with a 3.84 W input. Both DC fan speeds can be varied by directly adjusting the input voltages. A capillary tube with a 2.4 mm OD and 93 cm long is used as the expansion device.

3.2. System identification of THCS

Since the system dynamics of the THCS may be nonlinear, a linearly perturbed dynamics model is adopted which is derived from Eq. (4).

$$\begin{bmatrix} \tilde{T}_x \\ \tilde{H}_x \end{bmatrix} = \begin{bmatrix} G_{11}(s) & G_{12}(s) \\ G_{21}(s) & G_{22}(s) \end{bmatrix} \begin{bmatrix} \tilde{E}_o \\ \tilde{E}_i \end{bmatrix}, \tag{5}$$

where $\tilde{T}_x$ is the perturbed chamber temperature from an equilibrium value, i.e. $T_x(t) = \bar{T} + \tilde{T}(t)$; $\tilde{H}_x$ is the perturbed chamber humidity, i.e. $H_x(t) = \bar{H} + \tilde{H}(t)$; $\tilde{E}_o$ is the perturbed input voltage of the outer fan, i.e $E_o(t) = \bar{E}_o + \tilde{E}_o(t)$; $\tilde{E}_i$ is the perturbed input voltage of the inner fan, i.e. $E_i(t) = \bar{E}_i + \tilde{E}_i(t)$.

The system identification is performed to $G_{11}(s)$, $G_{12}(s)$, $G_{21}(s)$, and $G_{22}(s)$ separately using the input isolation method and step response test [5]. In identifying the model $G_{11}(s)$, only the input signal $\tilde{E}_i$ (inner fan driving voltage) is applied to the system while keeping $\tilde{E}_o = 0$ and the temperature response $\tilde{T}_x$ is measured. In identifying the model $G_{12}(s)$, only the input signal $\tilde{E}_o$ (outer fan driving voltage) is applied to the system while keeping $\tilde{E}_i = 0$ and the temperature $\tilde{T}_x$ is measured. A similar method is applied to the identification of the models $G_{21}(s)$ and $G_{22}(s)$.

Step response tests were performed in the present study. The step response data are first filtered by a low-pass filter. To identify the model $G_{11}(s)$, a step of $\tilde{E}_o$was applied and the temperature response $\tilde{T}_x$ was measured. By suddenly changing the outer fan voltage $\tilde{E}_o$ from a steady-state operation and measuring the response of chamber temperature $\tilde{T}_x$, we can obtain the dynamics model from the data analysis.

For a step change of $\tilde{E}_o(t) = K_o u(t), u(t)$ is the unit step function and $\tilde{E}_o(s) = K_o/s$. Taking the time derivative of $\tilde{E}_o(t)$, we have

$$\tilde{E}'_o(t) \equiv \frac{d\tilde{E}_o(t)}{dt} = K_o \delta(t). \tag{6}$$

Taking the Fourier transform of the time derivative of $\tilde{E}_o(t)$, we obtain

$$\tilde{E}'_o(j\omega) \equiv F\left[\frac{d\tilde{E}_o(t)}{dt}\right] = j\omega \tilde{E}_o(j\omega) = F[K_o \delta(t)] = K_o. \tag{7}$$

In the meantime, if we take the Fourier transform of the time derivative of the step response $\tilde{T}_x(t)$, we obtain

$$\tilde{T}'_x(j\omega) \equiv F\left[\frac{d\tilde{T}_x(t)}{dt}\right] = j\omega \tilde{T}_x(j\omega). \tag{8}$$

Combining Eqs. (7) and (8) we obtain

$$\frac{\tilde{T}'_x(j\omega)}{\tilde{E}'_o(j\omega)} = \frac{\tilde{T}_x(j\omega)}{\tilde{E}_o(j\omega)} = G_{11}(j\omega). \tag{9}$$

From Eq. (7), we further obtain

$$G_{11}(j\omega) = \frac{\tilde{T}'_x(j\omega)}{K_o}. \tag{10}$$

Eq. (10) depicts that the Fourier transform of the time derivative of the step response function dividing by K_o is the frequency response of the model $G_{11}(s)$.

The system identification is performed using a step input (voltage of inner or outer fans) to the THCS and measure the input and output (chamber temperature and humidity) signals simultaneously. Fig. 7 is a typical frequency response

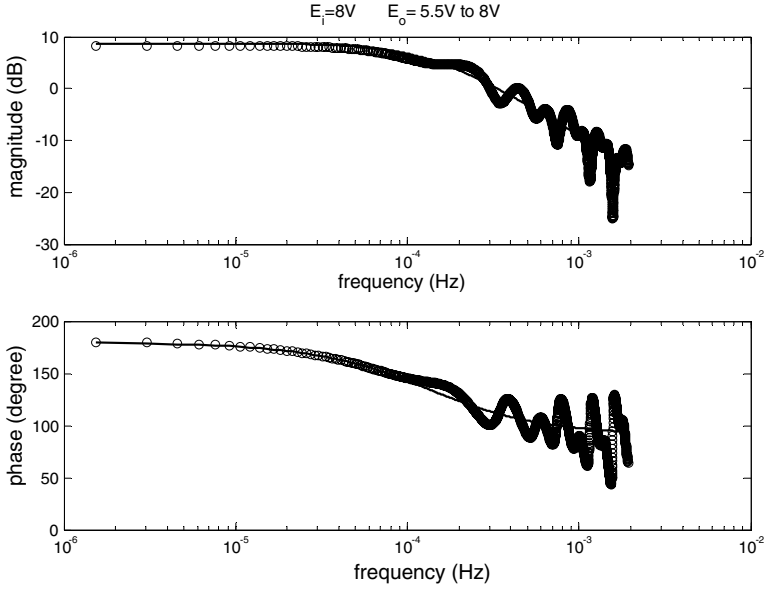

Fig. 7. Frequency response of $G_{11}(s)$ at $E_i = 8$ V.

Table 1
Identification of the model $G_{11}(s)$ at various E_i

Operating point	E_i (V)	E_o (V)	k	p
1	8	5.5 → 8	0.0023	0.00085
2	8	8 → 5.5	0.00186	0.00068
3	8	8 → 15	0.00089	0.002
4	8	15 → 8	0.00067	0.00152
5	10	5.5 → 8	0.00219	0.00091
6	10	8 → 5.5	0.00183	0.00073
7	10	8 → 15	0.00077	0.00173
8	10	15 → 8	0.00042	0.00094
9	12	5.5 → 8	0.00253	0.00113
10	12	8 → 5.5	0.00214	0.00078
11	12	8 → 15	0.00073	0.00134
12	12	15 → 8	0.00056	0.00122
Average model			0.00146	0.001

of the model $G_{11}(s)$ obtained from the test at $E_i = 8$ V and E_o imposed with a step change from 8 to 15 V. The results shown in Fig. 7 indicate that the phase of $G_{11}(j\omega)$ varies from 180° at a low frequency to approaching 90° at a high frequency and the gain of $G_{11}(j\omega)$ has a slope −20 db/decade. This indicates that the model $G_{11}(s)$ is probably of the first order.

$$G_{11}(s) = \frac{-k}{s+p}. \tag{11}$$

Fitting the experimental data to the model [6], we obtain the first order model (Eq. (11)) at various inner fan voltages E_i and the resulting k and p of the first order model are listed in Table 1. From Table 1, the average of the linearly perturbed system dynamics model $G_{11}(s)$ are obtained and shown in Fig. 8 with circles:

$$\bar{G}_{11}(s) = \frac{-0.00146}{s+0.001}. \tag{12}$$

Table 2
Identification of the model $G_{12}(s)$

Operating point	E_i	E_o	k	p
1	6 → 9	8	0.000399	0.00092
2	9 → 12	8	0.000562	0.00281
3	6 → 9	10	0	0
4	9 → 12	10	0	0
5	6 → 9	12	0	0
6	9 → 12	12	0.000071	0.00035
Average model			0.000197	0.0016

Repeating the above method, we obtain the rest of the models whose gain, poles and zeros are presented in Tables 2–4. Some of the identified gains K and poles p_1 with a zero value reveals that the chamber temperature is not affected by the inner fan speed variation for the outer fan voltage 10–12 V. It is noticeable that for the humidity response with respect to the outer fan voltage change, the identified model $G_{21}(s)$ as shown in Fig. 9, are a non-minimum phase system. This means that the chamber humidity will respond toward an opposite direction at the beginning of an input change.

The obtained average models are summarized as follows:

$$\bar{G}_{12}(s) = \frac{0.000197}{s+0.0016}, \tag{13}$$

$$\bar{G}_{21}(s) = \frac{-0.01086(s-0.000333)}{(s+0.00667)(s+0.00082)}, \tag{14}$$

$$\bar{G}_{22}(s) = \frac{0.008916(s+0.00062)}{(s+0.006478)(s+0.000844)}. \tag{15}$$

It is seen that the temperature response models, $G_{11}(s)$ and $G_{12}(s)$, are of a first order. The humidity response models, $G_{21}(s)$ and $G_{22}(s)$, are of a second order with a zero. The

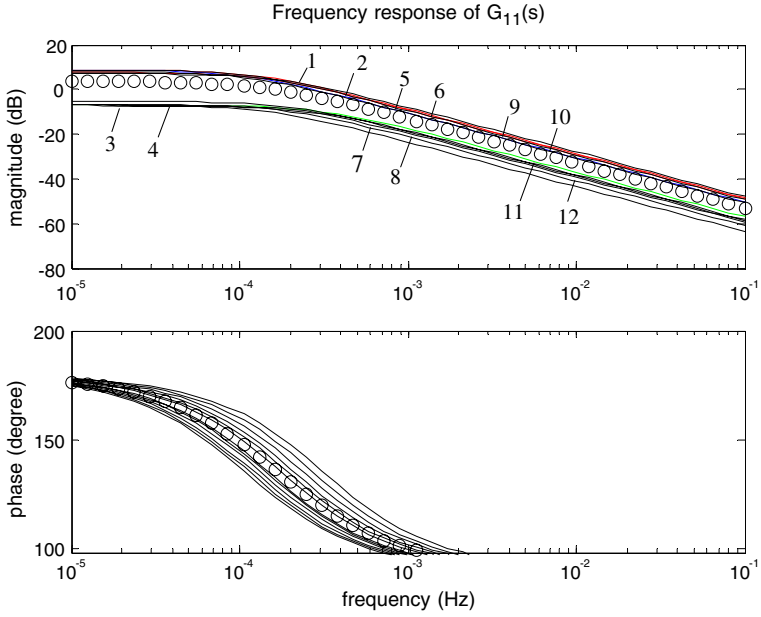

Fig. 8. Frequency response of $G_{11}(s)$ at various E_i.

Table 3
Identification of the model $G_{21}(s)$

Operating point	E_i (V)	E_o (V)	k	z	p_1	p_2
1	8	5.5 → 8	0.01243	0.00029	0.00632	0.00084
2	8	8 → 5.5	0.0145	0.000434	0.00646	0.00063
3	8	8 → 15	0.00573	0.000184	0.01048	0.00113
4	8	15 → 8	0.00731	0.00026	0.00333	0.00119
5	10	5.5 → 8	0.01528	0.000273	0.00651	0.00095
6	10	8 → 5.5	0.01575	0.000311	0.00723	0.00074
7	10	8 → 15	0.00557	0.000166	0.00805	0.00132
8	10	15 → 8	0.00804	0.000001	0.00622	0.00096
9	12	5.5 → 8	0.0101	0.000374	0.00422	0.00102
10	12	8 → 5.5	0.01036	0.000426	0.00488	0.00068
11	10	8 → 15	0.00499	0.000279	0.00889	0.00099
12	12	15 → 8	0.01548	0.000321	0.00912	0.00123
Average model			0.01086	0.000333	0.00667	0.00082

Table 4
Identification of the model $G_{22}(s)$

Operating point	E_i (V)	E_o (V)	k	z_1	p_1	p_2
1	6 → 9	8	0.013557	0.00033	0.00768	0.000624
2	9 → 12	8	0.004993	0.00236	0.003584 − 0.0028i	0.003584 − 0.0028i
3	6 → 9	10	0.013557	0.00047	0.00728	0.000659
4	9 → 12	10	0.00573	0.00235	0.003902 + 0.0032i	0.003902 − 0.0032i
5	6 → 9	12	0.010222	0.00053	0.0059	0.000812
6	9 → 12	12	0.006199	0.00041	0.00768	0.000624
Average model			0.008916	0.00062	0.006478	0.000844

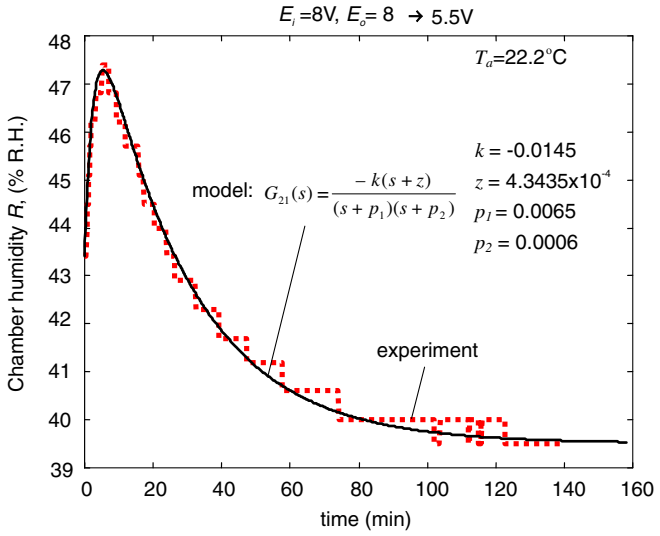

Fig. 9. Step response of the model $G_{21}(s)$.

average model of the THCS (Eqs. (12)–(15)) can be used in the control system design.

4. System control of a THCS

4.1. Control system design of a THCS

The control system for the THCS is basically a MIMO. In order to simplify the design, the MIMO dynamics of the

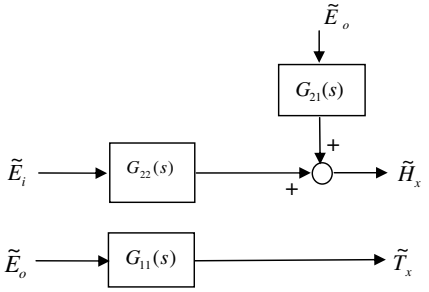

Fig. 10. Simplified system dynamics model of THCS.

THCS can be approximated by a single-input-single-output (SISO). From the average model (Eqs. (12)–(15)) we found that $|G_{11}(j\omega)| \gg |G_{12}(j\omega)|$. Hence, the system dynamic behavior of $G_{12}(s)$ can be ignored as shown in Fig. 10. That is,

$$\begin{bmatrix}\tilde{T}_x\\ \tilde{H}_x\end{bmatrix} = \begin{bmatrix}\frac{-0.00146}{s+0.001} & \frac{0.000197}{s+0.0016}\\ \frac{-0.01086(s-0.000333)}{(s+0.00667)(s+0.00082)} & \frac{0.008916(s+0.00062)}{(s+0.006478)(s+0.000844)}\end{bmatrix}\begin{bmatrix}\tilde{E}_o\\ \tilde{E}_i\end{bmatrix}$$
$$\cong \begin{bmatrix}\frac{-0.00146}{s+0.001} & 0\\ \frac{-0.01086(s-0.000333)}{(s+0.00667)(s+0.00082)} & \frac{0.008916(s+0.00062)}{(s+0.006478)(s+0.000844)}\end{bmatrix}\begin{bmatrix}\tilde{E}_o\\ \tilde{E}_i\end{bmatrix}.$$

Hence,

$$\tilde{T}_x = G_{11}(s)\tilde{E}_o, \quad (16)$$
$$\tilde{H}_x = G_{21}(s)\tilde{E}_o + G_{22}(s)\tilde{E}_i. \quad (17)$$

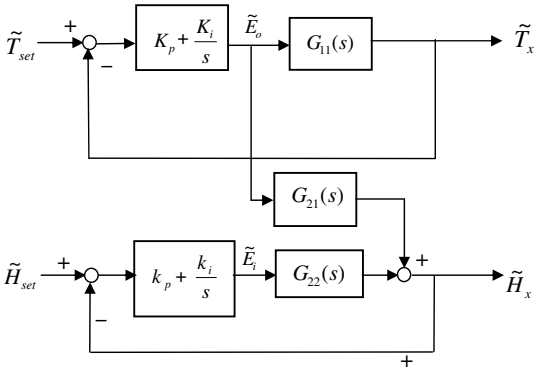

Fig. 11. Decoupled feedback control system of THCS.

The feedback control system of the THCS is thus simplified to Fig. 11, for the PI controller. The control system design can then be separated. For chamber temperature control, it becomes a single-loop system, i.e. temperature control loop. For humidity control, it can also be treated as a single-loop with a disturbance input from the temperature control loop. The control of the THCS is thus decoupled into two individual single loops. In the humidity control loop, the variation of the outer fan voltage which is mainly for temperature control can be treated as a disturbance which can be rejected to some extent from a careful design of the PI controller. This makes the control system very simple.

We define the feedback system characteristics according to the requirement in a practical application. For the temperature control loop, the specification is defined as

(1) rise time <1200 s;
(2) overshoot <10%;
(3) steady-state error <±0.5 °C.

For the humidity control loop, the specification is defined as

(1) rise time <300 s;
(2) overshoot <5%.

The control system analysis was carried out using the root-locus method to find the parameters of the PI controllers. For the temperature control loop, we obtain $K_P = 2.4$ and $K_i = 0.0045$. For the humidity control loop, we obtain $k_i = 0.01$ and $k_p = 10.9$.

4.2. Control system implementation on a THCS

The control system obtained from the above analysis is implemented digitally using a PC. HT-734-M-06 is adopted as the temperature and humidity sensor. A YOKOGAWA HR1300 recorder was used to measure the temperature and humidity and communicate with a PC. The controller output signal is sent to HR1300 and

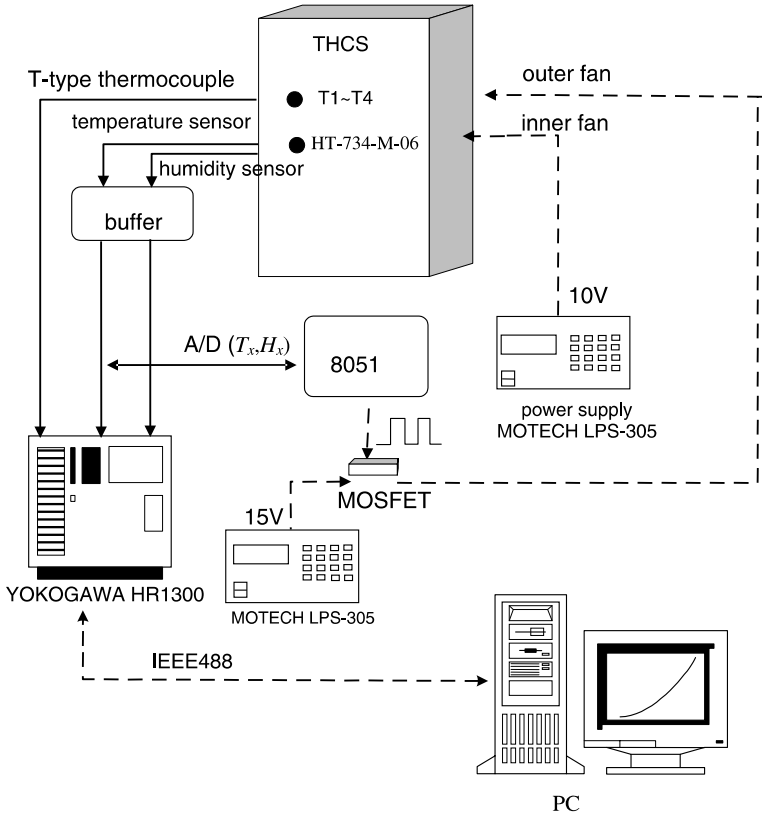

Fig. 12. Schematic of control system implementation.

then a 8051 microprocessor. 8051 receives the command and generates a PWM signal to a MOSFET (IRFP 450) to adjust the voltages for the inner and outer fans. The control system design is shown in Fig. 12.

4.3. System test for single-loop temperature control

The first test is performed for the single-loop temperature control only. Fig. 13 shows the temperature response for a chamber temperature setting change from 22 to 19 °C, with a constant inner fan voltage $E_i = 10$ V. It takes about 20 min to reach a steady-state with an error of $<\pm 0.1$ °C. The single-loop temperature control with a heat load disturbance of 10 W was then carried out to determine the capability of disturbance rejection of the control system. A heat input using a light bulb (10 W) installed inside the chamber was applied when the system is steady at a fixed inner fan voltage (10 V) and chamber setting temperature (20 °C). Fig. 14 shows that the chamber temperature is kept at 20 ± 0.5 °C during the transient right after the presence of the disturbance and the target value (20 °C) is restored within 30 min of the disturbance. For a larger heat load disturbance of 20 W, the control signal has a saturation which will trigger the reset of the integral control. Fig. 15 shows that the chamber temperature is kept at 20 ± 1.0 °C during the transient right after the presence of a disturbance and the target value (20 °C) is restored within 50 min of the disturbance. The longer time is due to the saturation of the control system. The quality of the control system is shown satisfactorily in temperature regulation as well as disturbance rejection.

4.4. System test for simultaneous temperature and humidity control

The next test is performed for simultaneously temperature and humidity control. The chamber temperature is set to 20 °C after a steady-state performance at 22 °C and the humidity is set to 40% R.H. after a steady value 45% R.H. Fig. 16 shows that the temperature is controlled to within 20 ± 0.1 °C with a rise time of about 35 min. The chamber humidity is controlled to within $40 \pm 1\%$ R.H. with a rise time of about 5 min. The humidity control reacts faster than the temperature control due to the larger and faster control signal of the inner fan voltage. Physically, the inner fan speed change will result in a faster response of chamber humidity if the evaporator temperature was kept within a narrow range. The outer fan speed

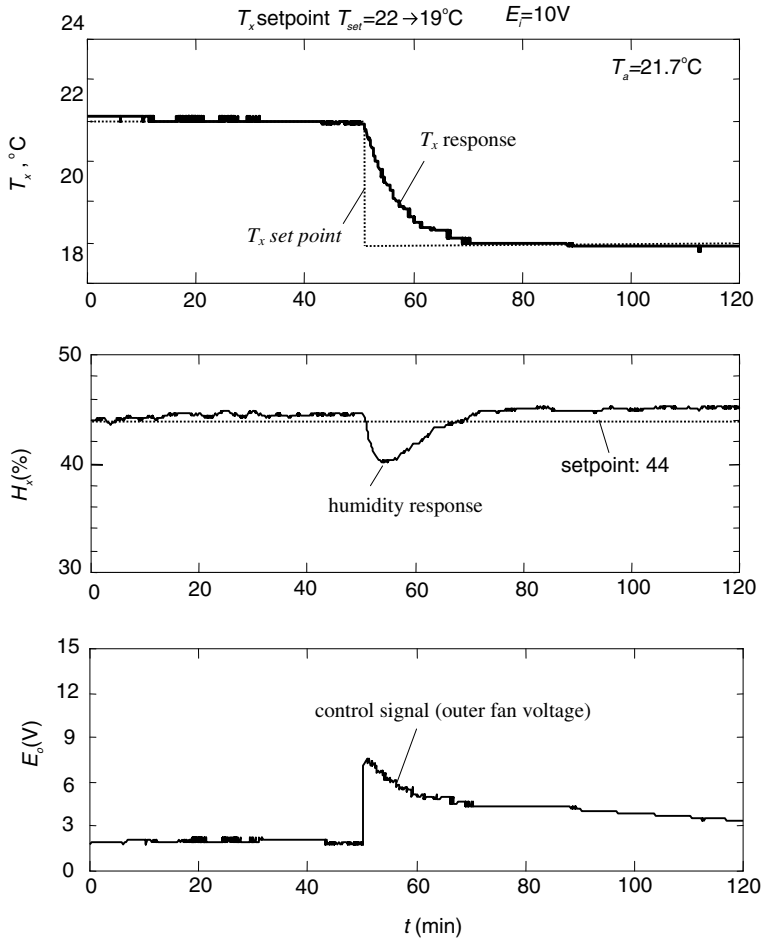

Fig. 13. Temperature step response test.

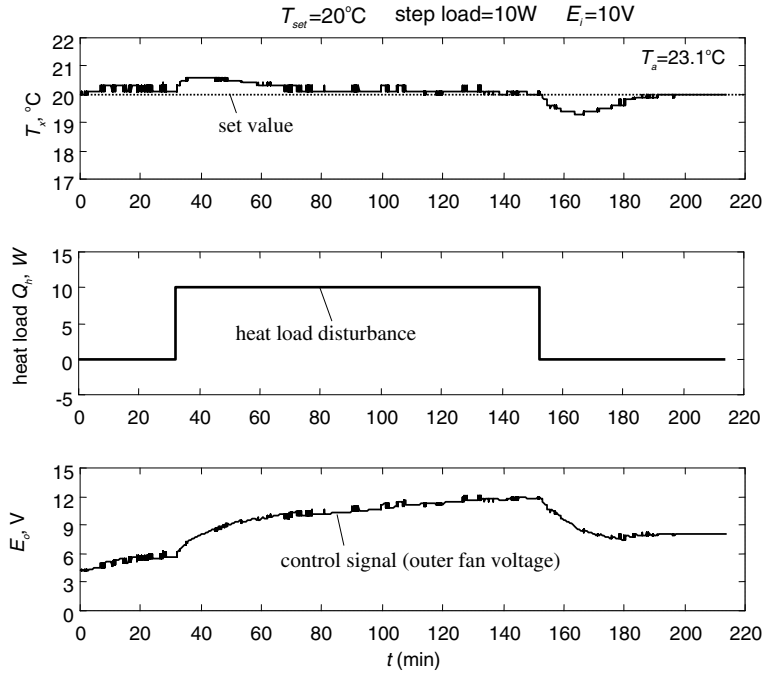

Fig. 14. Test of single-loop temperature control with a heat disturbance of 10 W.

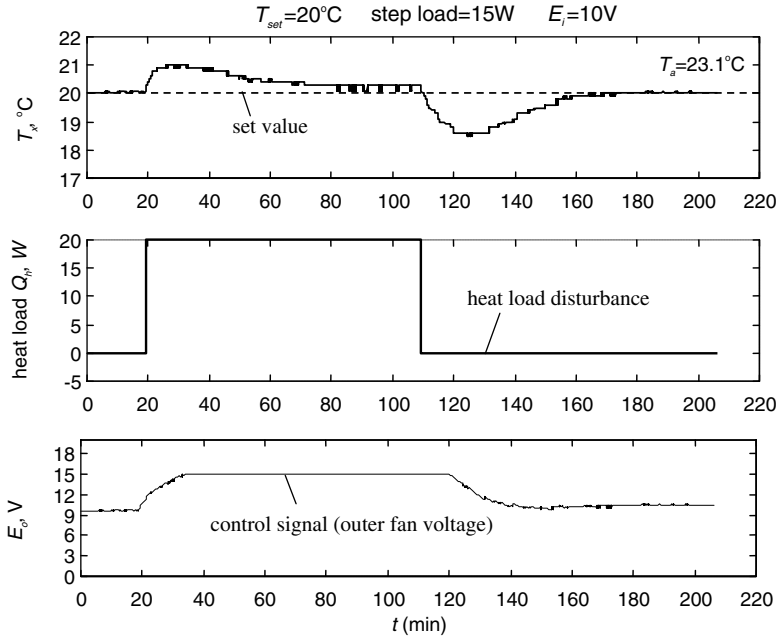

Fig. 15. Test of single-loop temperature control with a heat load disturbance of 20 W.

variation will easily cause an overshoot because the cooling capability and dehumidification process are related to the vapor compression cycle performance. Thus, the control system is designed to suppress the overshoot (<10%) which causes the control signal to the outer fan (E_o) to change more smoothly than the inner fan (E_i) as shown in Fig. 16.

We also performed a system test with a heat load disturbance of 20 W to show the robustness of the control system for simultaneous temperature and humidity control. Fig. 17 shows that it takes about 60 min to restore the chamber temperature to the set value in the presence of a 20W heat load disturbance. This is due to the fact that the outer fan runs at saturation (15 V) for about 20 min. The chamber temperature variation at the disappearance of the heat load disturbance however ends up only for about 25 min. The humidity control however is almost

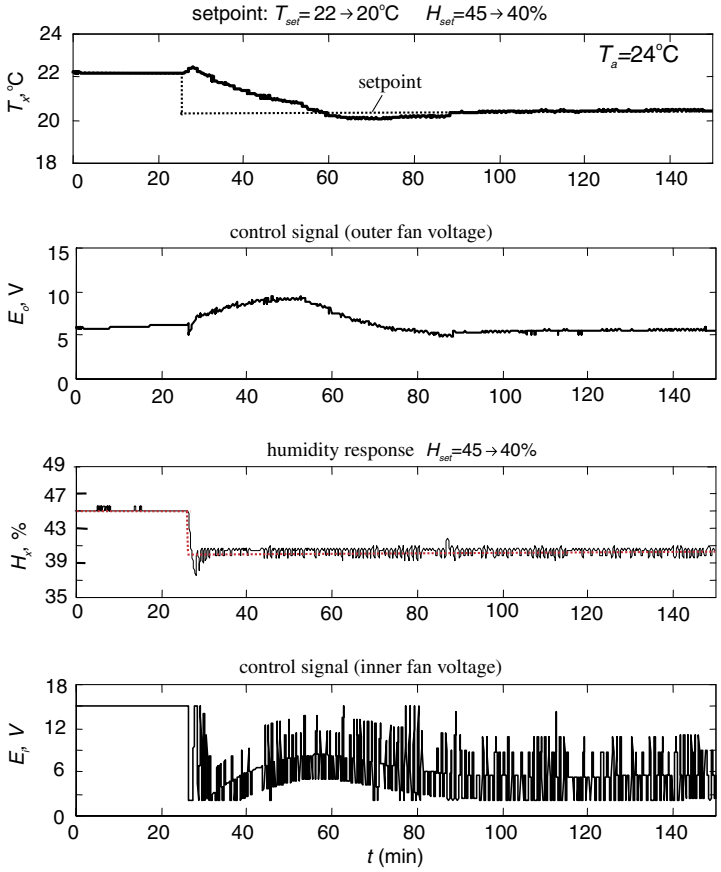

Fig. 16. Multivariable control results.

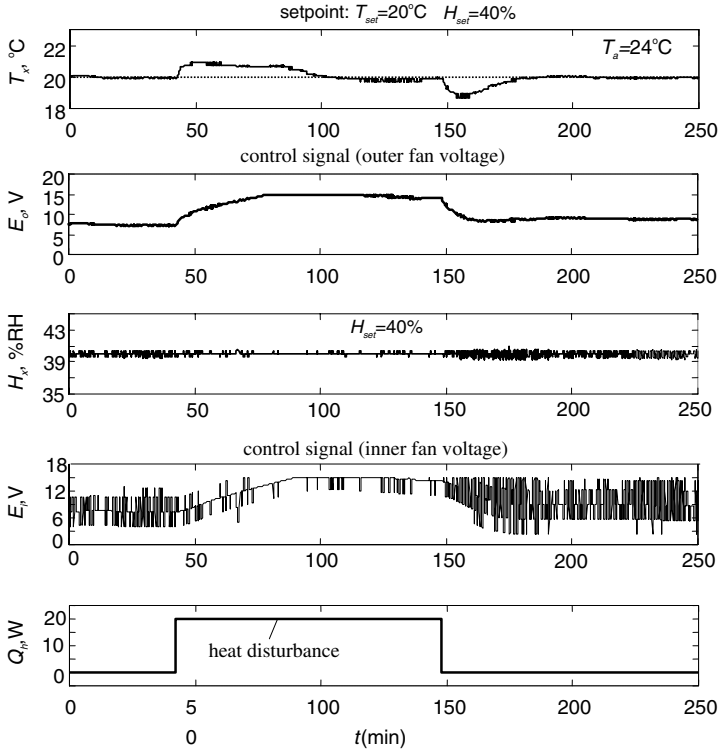

Fig. 17. Multivariable control with a heat load disturbance of 20 W.

not influenced by the heat load disturbance since the inner fan speed or voltage (E_i) varies more rapidly, although also associated with saturation. Both the chamber temperature and humidity are shown to be able to remain at the setting values with negligible errors even in the presence of a heat load disturbance.

Increasing the magnitude of the heat load disturbance will result in the system going out-of-control due to the machine operating limit. Experimental results show that a heat load disturbance larger than 50 W will result in a steady-state error higher than 0.5 °C for the temperature control. Therefore, 50 W is the maximum heat load for the THCS. This is reasonable since the rated power input of the compressor is 250 W.

5. Discussions and conclusion

A conventional temperature and humidity control includes the processes of cooling, dehumidification and reheating process. This makes the equipment very sophisticated with a low energy efficiency. The present study develops a direct temperature and humidity control system (THCS) in which the condenser is divided into two parts. By properly adjusting the fan speeds of the outer and inner condensers, the net heating or cooling of the chamber and the temperature and humidity control can be achieved. The temperature and humidity control of the present design thus follows a direct process.

The system dynamics of the THCS is basically a MIMO. System identification is first carried out to determine the system dynamics model of the THCS using the step response test. The temperature response models, $G_{11}(s)$ and $G_{12}(s)$, are shown to be of first order. The humidity response models, $G_{21}(s)$ and $G_{22}(s)$, are of second order with a zero. The average models of the THCS (Eqs. (12)–(15)) are used in the control system design. The present study found that the MIMO dynamics of the THCS can be approximated by a two single-input-single-output (SISO) system. The control system design can then be decoupled into a temperature control loop and a humidity control loop. In the humidity control loop, the variation of the outer fan voltage which is mainly for temperature control can be treated as a disturbance which can be rejected to some extent from a careful design of the controller. This makes the control system design very simple. We developed a control system using a PI controller and performed a design analysis. The implementation of the control system on a PC with a 8051 microprocessor has experimentally shown that the control system provides an accurate control for both temperature and humidity in the presence of a heat load disturbance.

The chamber temperature and humidity can be controlled to within ±0.1 °C and ±1% R.H. accuracy, respectively. In the presence of a heat load disturbance, the controller can restore the THCS to operate at the setting values within a reasonable transient time. Experimental results show that the maximum heat load disturbance for the THCS is 50 W. The maximum heat load can be further improved by modifying the vapor compression cycle or changing the fans with a larger capacity. The results of the present study can be applied in a larger system, such as an industrial process, to provide a simple temperature and humidity control.

Acknowledgement

The present study was supported by the National Science Council, Taiwan, through Grant No. NSC91-2212-E-002-077.

References

[1] C. Rentel-Gomez, M. Velez-Reyes, Decoupled control of temperature and relative humidity using a variable-air-volume HVAC system and non-interacting control, in: IEEE Conference on Control Applications – Proceedings, 2001, pp. 1147–1151.
[2] Y. Zhong, J. Yang, J. Deng, Multivariable fuzzy control of temperature and humidity in a greenhouse, Nongye Jixie Xuebao/Trans. Chinese Soc. Agr. Mach. 32 (3) (2001) 75–78.
[3] A. Kimbara, M. Kasahara, K. Shigeru, K. Kamimura, T. Matsuba, Y. Atsushi, Modeling of an environmental chamber, ASHRAE Trans. 1 (1995) 262–273.
[4] Carios A. Smith, Armando B. Corripio, Principles and Practice of Automatic Process Control, John Wiley & Sons, NewYork, 1985.
[5] B.J. Huang, S.B. Wang, Identification of solar collector dynamics using physical model-based approach, Trans. ASME J. Dyn. Syst. Meas. Contr. 116 (1994) 755–763.
[6] H. Rake, Step response and frequency response methods, Automatica 16 (1980) 519–526.